Submitted to *Ceramics International* as a *Short Communication*, September 2022. Revised November 2022

Solid-state spark plasma sintering of super wear resistant B_4C–SiC–TiB_2 triplex-particulate composites

Fernando Rodríguez-Rojas, Victor Zamora, Fernando Guiberteau, Angel L. Ortiz *

Departamento de Ingeniería Mecánica, Energética y de los Materiales,
Universidad de Extremadura, 06006 Badajoz, Spain.

Abstract

B_4C–SiC–TiB_2 ceramic composites with equal volume fractions of the three phases (*i.e.*, 1B_4C–1SiC–1TiB_2) were fabricated by solid-state spark-plasma sintering (SPS) from commercially available B_4C, SiC, and TiB_2 powders, first optimizing their densification temperature and then investigating for the first time the unlubricated sliding wear of the optimally SPS-ed composite. It is shown that SPS is optimal at 1800°C (under 75 MPa pressure and 5 min soaking), which is much lower than the temperatures used so far for both the solid-state hot-pressing and SPS of this and other B_4C–SiC–TiB_2 composites. It is also shown that the optimally SPS-ed 1B_4C–1SiC–1TiB_2 composite has a triplex-particulate microstructure with evenly distributed carbide and boride grains whose sizes are essentially those of the corresponding starting powders, and that it is ultrahard (*i.e.*, ~35 GPa) and relatively tough (*i.e.*, ~4 MPa·$m^{1/2}$). Moreover, it is demonstrated that, due to its ultra-high hardness and proneness to form a coherent oxide tribolayer, it is also very immune to wear, possessing an unprecedented super wear resistance to unlubricated sliding contact (*i.e.*, ~$1.6 \cdot 10^8$ (N·m)/mm^3), thanks to which it only undergoes very mild abrasion in the form of superficial plastic scratches with hardly any material removal by micro-fracture. Finally, implications of interest for the ceramics and hard-materials communities

are discussed.

Keywords: Ceramic composites; Ultrahard materials; Wear; Spark plasma sintering; Borides/carbides.

* Corresponding author: Angel L. Ortiz (alortiz@unex.es)

1. Introduction

Multi-particulate ceramic composites based on a combination of covalent or interstitial carbides and interstitial borides constitute a recent class of structural materials with great appeal for contact-mechanical and tribological applications [1-5]. This is because their carbide and boride constituents make them super-hard and super-strong, while their multi-particulate microstructures make them tougher than the corresponding monolithic ceramics. Among the many possible carbide–boride composites, those triplex-particulate composites with B_4C and SiC as two of their three phases are especially interesting because they are both extremely hard and lightweight, especially B_4C, and, in addition, SiC provides oxidation resistance [6]. Having a transition metal diboride (TMB_2) as the third phase is also very desirable because these borides are very hard too, as well as extremely refractory, highly stable chemically, and with much higher thermal expansion coefficients than B_4C and SiC [7]. In particular, TiB_2 stands out because it is much lighter, harder, and tougher than the rest of the TMB_2, and therefore yields more appealing triplex-particulate composites [5].

B_4C–SiC–TiB_2 triplex-particulate composites have already been solid-state sintered from commercially available B_4C, SiC, and TiB_2 powders with very varied fractions of the three phases, by both hot-pressing (HP) [5,8,9] and spark-plasma sintering (SPS) [10,11]. These studies confirmed the expectations, demonstrating that the B_4C–SiC–TiB_2 composites are a family of extraordinarily-hard materials [5,8-11], and also super strong with flexural strength close and even higher than 1000 MPa depending on their phase composition (for example, ~927 MPa for $1B_4C$–1SiC–$1TiB_2$ composites and ~1325 MPa for $15B_4C$–15SiC–$70TiB_2$ composites) [5,9]). Indeed, detailed Vickers indentation tests on $1B_4C$–1SiC–$1TiB_2$ and $15B_4C$–15SiC–$70TiB_2$ composites (compositions given in volume fractions) have shown that they possess an impressive ultra-hardness that increases from ~33 GPa and ~31 GPa at 19.6 N up to ~54 GPa and ~44 GPa at 0.49

N [5,9], respectively, trends that are thought valid for any B_4C–SiC–TMB_2 composite [5]. With this remarkable hardness, the B_4C–SiC–TiB_2 composites should also be little susceptible to wear, and therefore very appealing tribo-components. Surprisingly however, wear of B_4C–SiC–TiB_2 composites has not yet received attention despite the fact that tribological applications concentrate a large part of the demand for hard materials.

Also importantly, a major concern of the B_4C–SiC–TiB_2 composites is that their current fabrication by both solid-state HP and SPS from B_4C+SiC+TiB_2 powders is very demanding (*i.e.*, generally HP cycles at 1950°C–2000°C lasting hours [5,8,9] and SPS cycles, although much shorter, still at 1950°C [10] or 2000°C [11]). Their fabrication by reactive HP, from for example B_4C+TiC+Si [12,13], B_4C+Ti_3SiC_2 [14], and B_4C+Ti+Si [15] powders, is equally demanding (*i.e.*, cycles at 1850°C–2100°C lasting hours), but it is less so by reactive SPS, from for example B_4C+$TiSi_2$ [16] and B_4C+Ti_3SiC_2+Si [17-19] powders (*i.e.*, cycles at 1650°C–1800°C lasting minutes). Unfortunately however, reactive SPS allows only a more reduced compositional design of B_4C–SiC–TiB_2 composites than solid-state SPS, and, in addition, these do not have homogeneous triplex microstructures (*i.e.*, evenly dispersed B_4C, SiC, and TiB_2 grains) but heterogeneous microstructures (*i.e.*, B_4C grains plus clusters of SiC+TiB_2 grains). SPS [20], whose industrial implementation has growth considerably over the last decade, is widely used today to densify refractory monolithic ceramics and ceramic composites that would otherwise be difficult or impossible to densify by pressureless sintering or HP, and to do so with more refined microstructures due to ultrafast densification cycles at lower temperatures. Therefore, it surprises that no attempts have been made so far to smooth the solid-state SPS temperature of the B_4C–SiC–TiB_2 composites, which has not been investigated as a processing variable in the earlier studies, especially because wear resistance and strength of polycrystalline ceramics benefit from microstructural refinement [21,22].

With these premises in mind, the purpose of the present study was to examine these two pending issues using as a referent the B_4C–SiC–TiB_2 composite with equal volume fractions of the three phases (hereafter termed 1B_4C–1SiC–1TiB_2 composite), evaluating both (*i*) its lower-temperature SPS densifiability and (*ii*) especially its tribological potential under unlubricated sliding contact (which is a very common type of frictional contact).

2. Experimental procedure

The starting materials were commercially available powders (H.C. Starck, Germany) of B_4C (d_{50} ~0.3–0.6 μm; ρ ~2.51 g/cm^3; Grade HD-20), α-SiC (d_{50} ~0.55 μm; ρ ~3.23 g/cm^3; UF-15), and TiB_2 (d_{50} ~2.5–3.5 μm; ρ ~4.5 g/cm^3; Grade F), which are composed of equiaxed particles. A powder batch was prepared by first combining the B_4C, SiC, and TiB_2 powders in equal volume fractions, next homogenizing them by wet ball-mixing in abundant methanol (*i.e.*, 100 g/l) for 24 h with Si_3N_4 balls, then drying the resulting slurry under continuous stirring, and finally de-agglomerating (but not sieving) the dried powders.

Subsequently, the B_4C+SiC+TiB_2 powder mixture was loaded into graphite dies (2.5-cm diameter) lined with graphite foils and covered by graphite blankets, and was consolidated by SPS (HP-D-10, FCT Systeme GmbH, Germany) in dynamic vacuum at 1600°C, 1700°C, 1800°C, or 1900°C (as measured by an axial pyrometer and reached at 100°C/min) for 5 min under 75 MPa pressure (applied at 300°C). The resulting 1B_4C–1SiC–1TiB_2 composites were ground and diamond polished to a 0.25-μm finish using conventional ceramographic procedures, and were characterised (*i*) microstructurally by water immersion porosimetry (*i.e.*, by the Archimedes method), scanning electron microscopy (SEM; S3600N, Hitachi, Japan), and X-ray diffractometry (XRD; D8 Advance, Bruker AXS, Germany), as well as (*ii*) mechanically (*i.e.*, hardness and

fracture toughness [23-25]) by Vickers indentation tests (MV-1, Matsuzawa, Japan) at 9.8 N load.

The optimally SPS-ed $1B_4C–1SiC–1TiB_2$ composite was characterised tribologically by sliding-wear tests in the ball-on-disk configuration. The tests were performed, in duplicate, under unlubricated conditions, at 40 N load, 10 cm/s linear sliding speed, 2 mm track radius, and 1000 m total sliding distance, using a diamond-coated SiC ball (Dball G10, Nova Diamant, UK) as counter-ball to simulate the worst scenario of sliding wear against a harder counterpart (according to the manufacturer's specifications, the ball hardness is >80 GPa). The worn surfaces of the $1B_4C–1SiC–1TiB_2$ disks were cleaned and examined by optical profilometry (OP; Profilm 3D, Filmetric, USA) to compute the worn volume and thence the specific wear rate (SWR) and the wear resistance, and by optical microscopy (OM; Epiphot 300, Nikon, Japan) and SEM to inspect the wear damage at the macroscopic and microscopic scales, respectively. The worn surface of the diamond-coated SiC counter-ball was also cleaned, and examined by OM.

3. Results and discussion

Figure 1 shows SEM images, taken with secondary electrons, representative of the fracture surface of the $1B_4C–1SiC–1TiB_2$ composite SPS-ed at 1600°C–1900°C for 5 min under 75 MPa, whose theoretical density calculated by the rule-of-mixture is ~3.596 g/cm^3. It can be seen in Fig. 1A that SPS at 1600°C was insufficient to achieve complete densification, resulting in a moderately porous composite that, according to the density measurements (*i.e.*, ~3.31 g/cm^3), is only ~92% dense. Moreover, it can be seen in Fig. 1B that SPS at 1700°C was also insufficient, leading to a slightly porous composite with a relative density measured of ~96.2% (*i.e.*, ~3.46 g/cm^3). Lastly, it can be seen in Figs. 1C-D that SPS at 1800°C or above already yielded fully dense composites (*i.e.*, 100% dense), a fact that the density measurements confirmed (*i.e.*, ~3.59–3.60 g/cm^3).

Importantly, SPS at 1800°C entails a notable reduction of 200°C and 150°C relative to the typical solid-state HP and SPS cycles previously used to fabricate $B_4C–SiC–TiB_2$ composites, respectively.

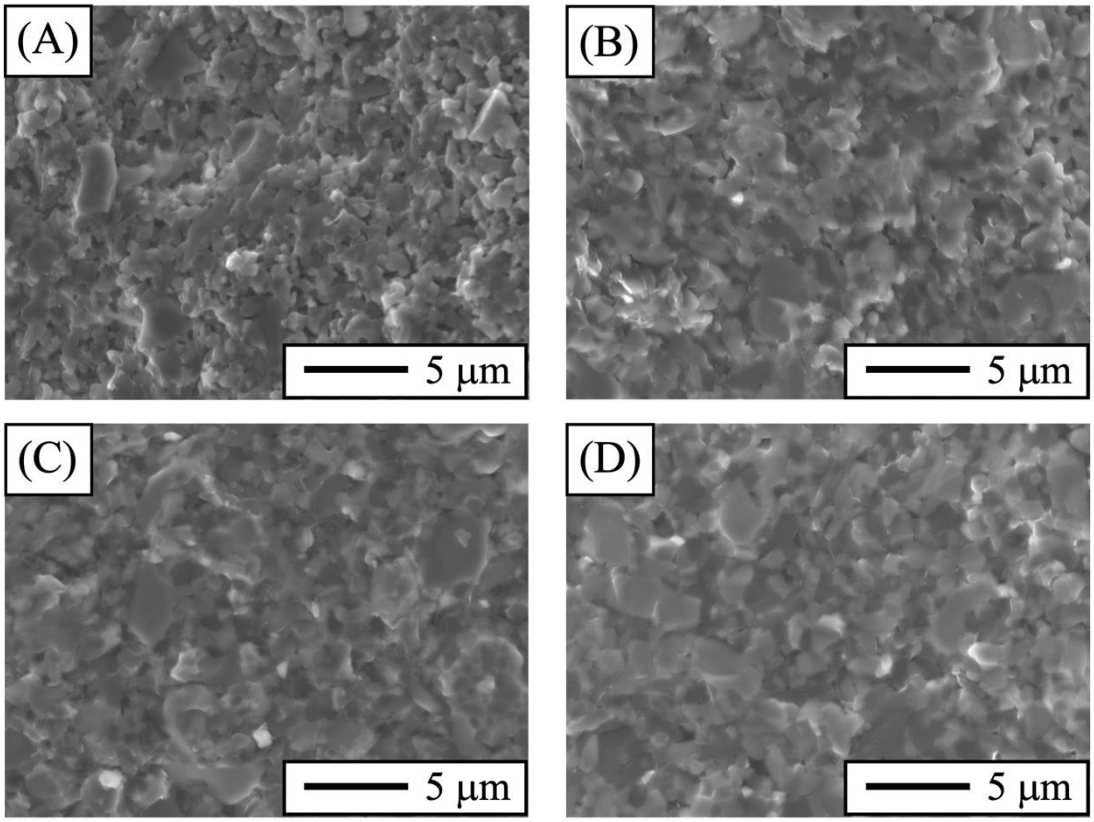

Figure 1. *SEM micrographs, taken with secondary electrons at 10 kV with no thermal or chemical etching, representative of the fracture surface of the $1B_4C–1SiC–1TiB_2$ composite SPS-ed for 5 min under 75 MPa at (A) 1600°C, (B) 1700°C, (C) 1800°C, and (D) 1900°C. Pitted zones in (C)-(D) are not pores, but small grains pulled-out during fracture.*

Figures 2A-D show the same SEM images as in Fig. 1 but taken with backscattered electrons. It can be seen that these $1B_4C–1SiC–1TiB_2$ composites have triplex-particulate microstructures, with a homogenous distribution of submicrometre B_4C (dark phase), submicrometre SiC (grey phase), and micrometre TiB_2 (white phase) grains. This is also evident in Figs. 2E-F, which show, by way of example, an SEM image representative of the polished surface of the $1B_4C–1SiC–1TiB_2$ composite SPS-ed at 1800°C. Hence, the microstructural scale of

the SPS-ed composites resembles the granulometry of the corresponding starting powders, indicating that there was limited grain growth during SPS. This, which is attributable to the lower-temperature ultrafast sintering, is important because it opens the door to obtaining the fine-grained microstructures that are so preferable in terms of wear resistance and strength [21,22]. For example, it is suggested that more refined microstructures could be achieved by using finer commercially available starting powders, ideally nano-powders, or by subjecting them to high-energy (co)ball-milling prior to SPS. Figure 3 shows the XRD patterns of the four composites fabricated. It can be seen that they are composed only of B_4C, SiC, and TiB_2, because C is a trace impurity of the B_4C starting powder, which rules out the occurrence of reaction between these carbides and boride during SPS. This is also important because it indicates that solid-state SPS can be used to fabricate B_4C–SiC–TiB_2 composites with on-demand compositions simply by controlling the powder batch formulation.

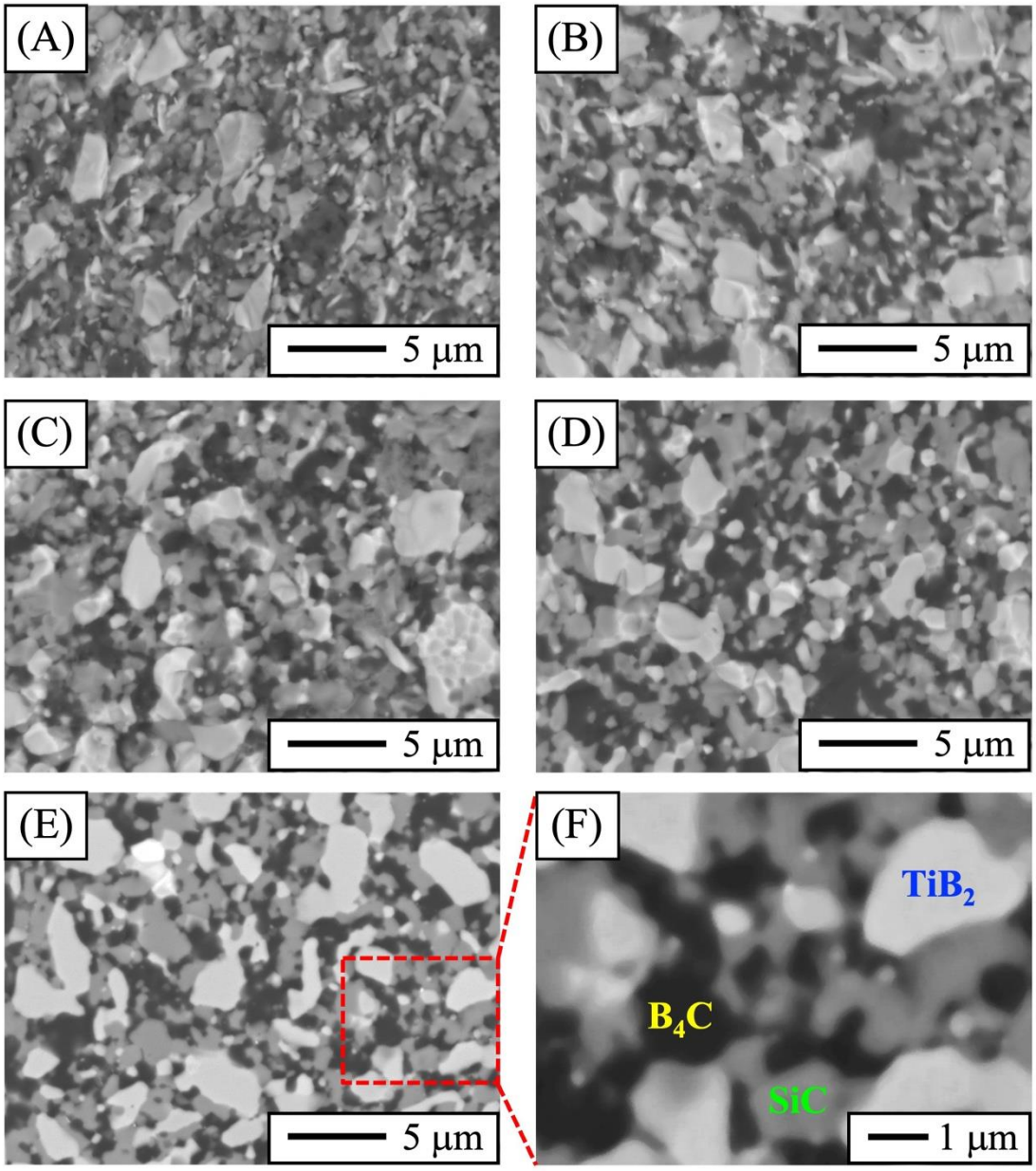

Figure 2. *SEM micrographs, taken with backscattered electrons at 10 kV with no thermal or chemical etching, representative of the fracture surface of the $1B_4C–1SiC–1TiB_2$ composite SPS-ed for 5 min under 75 MPa at (A) 1600°C, (B) 1700°C, (C) 1800°C, and (D) 1900°C, as well as (E)-(F) of the polished surface of the $1B_4C–1SiC–1TiB_2$ composite SPS-ed at 1800°C.*

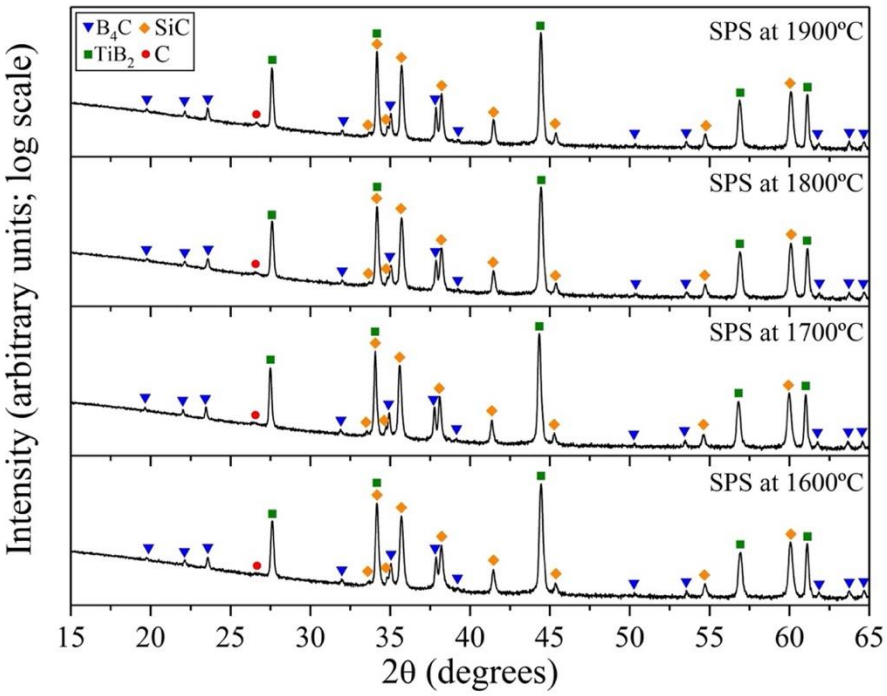

Figure 3. *XRD patterns, acquired with pure CuKα$_1$ incident radiation, of the 1B$_4$C–1SiC–1TiB$_2$ composite SPS-ed for 5 min under 75 MPa at 1600°C, 1700°C, 1800°C, and 1900°C, as indicated. Peak assignations, performed using the PDF2 database, are included. The intensity scale is logarithmic to facilitate observation of the weaker peaks.*

Figure 4 shows the hardness and toughness, as measured by Vickers indentation tests, of the 1B$_4$C–1SiC–1TiB$_2$ composite as a function of its SPS temperature. It can be seen that all four composites fabricated are superhard (*i.e.*, >20 GPa) or ultrahard (*i.e.*, >30 GPa), attributable to their composition with two covalent carbides (*i.e.*, B$_4$C and SiC) and a transition metal diboride (*i.e.*, TiB$_2$). The hardest ones (*i.e.*, ~35 GPa) are those SPS-ed at 1800°C and 1900°C because they are fully dense, while those SPS-ed at 1600°C and 1700°C are softer, albeit still extremely hard (*i.e.*, ~26 and 33 GPa, respectively), because they are, to a greater or lesser extent porous (*i.e.*, ~8% and 3.7%, respectively). It can also be seen that, despite their non-coarse-grained microstructures, all four are relatively tough (*i.e.*, ≥4 MPa·m$^{1/2}$), attributable mostly to toughening by the TiB$_2$ grains [5,9-11], and that they are essentially equally tough (4.0–4.4 MPa·m$^{1/2}$) because of their microstructural similarity and same composition. Specifically, toughening is mostly because the residual stresses induced by the thermoelastic mismatch between the uniformly distributed TiB$_2$

and B_4C/SiC grains result in homogeneous triplex microstructures with weak interfaces that favour crack deflection and bridging [10]. Note that the composite SPS-ed at 1600°C seems perhaps slightly tougher, but that this is simply an experimental artefact resulting from its ~8% porosity (*i.e.*, part of the mechanical energy is consumed in densifying the indented zone and is not therefore available to propagate the cracks). The optimal composite is thus the one SPS-ed at 1800°C, which has an unusual combination of ~35 GPa hardness and ~4 MPa·m$^{1/2}$ toughness and the lowest possible SPS temperature. Importantly, fabricating these composites by solid-state SPS is thus more recommendable than by solid-state HP because there are no hardness and toughness differences between the resulting materials (*i.e.*, ~35 GPa and ~4.0 MPa·m$^{1/2}$ *vs* ~33 GPa and ~4.5 MPa·m$^{1/2}$), but SPS is (*i*) much more energy efficient, and therefore cost effective, and (*ii*) more suitable to obtain fine-grained microstructures than HP because it uses smoother/faster densification cycles (*i.e.*, 1800°C for 5 min).

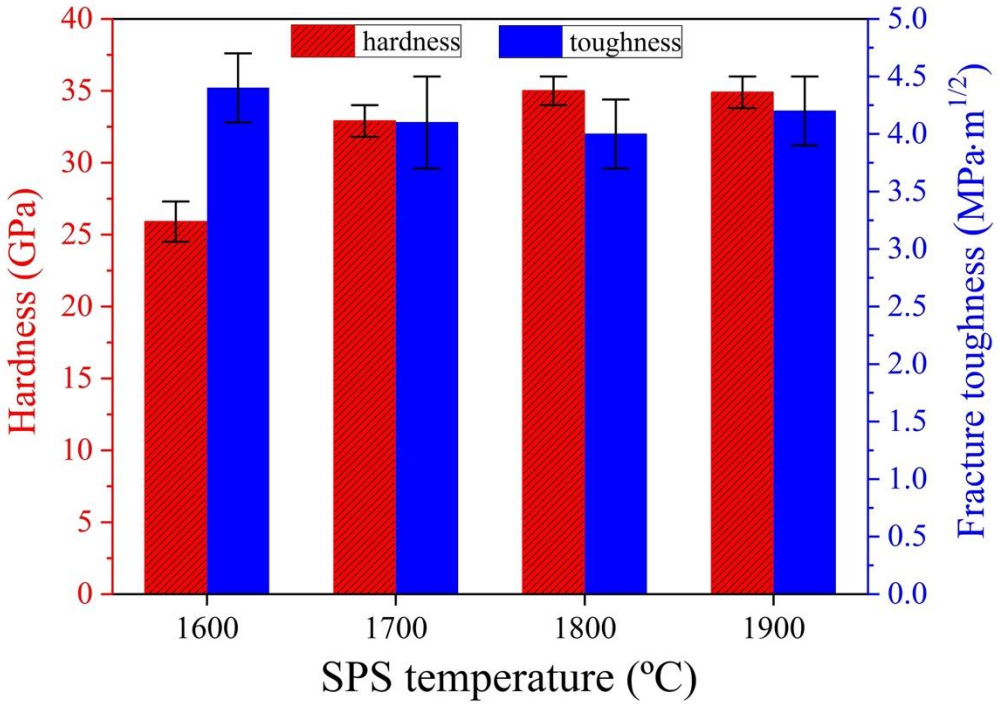

Figure 4. *Hardness and fracture toughness, determined by Vickers indentation tests, of the 1B_4C–1SiC–1TiB_2 composite SPS-ed for 5 min under 75 MPa at 1600°C, 1700°C, 1800°C, and 1900°C, as indicated. Mean values and standard deviations of 10 separate tests at 9.8 N are reported.*

Figure 5 shows relevant wear results for the $1B_4C–1SiC–1TiB_2$ composite SPS-ed at 1800°C, which, as mentioned above, is the optimal one. It can be seen in Fig. 5A that the coefficient of friction is very low (*i.e.*, <0.06 after the run-in stage) and smooth, in principle indicative that there was little wear. Certainly, Fig. 5B shows an OP 3-D image representative of the worn surface of this composite at the conclusion of the wear tests, where it is very evident that the residual wear track is very narrow (*i.e.*, ~205 μm) and extremely shallow (*i.e.*, ~0.37 μm). The wear volume computed from representative OP 2-D profiles extracted from that and other OP 3-D images, such as the one also shown by way of example in Fig. 5B, is indeed as low as ~0.00025(2) mm^3, which gives a minimum SWR of only ~$6.3(6)\cdot10^{-9}$ $mm^3/(N\cdot m)$ that classed its wear as very mild [26-28] despite it slid against a more ultra-hard counterpart (*i.e.*, diamond). This $1B_4C–1SiC–1TiB_2$ composite thus possesses a super wear resistance as high as ~$1.6(2)\cdot10^8$ $(N\cdot m)/mm^3$ that labels it as highly immune to wear. Consistently with this, Figs. 5C and 5D show OM and SEM images, respectively, representative of the worn surface, demonstrating that it remains largely intact, and that the little existing wear damage is essentially in the form only of superficial scratches (Fig. 5C), typical of plastic grooves, parallel to the sliding direction, with almost no material removal by micro-fracture (Fig. 5D). This pattern of macro- and micro-damage indicates that the minimum wear of the $1B_4C–1SiC–1TiB_2$ composite was the result of a very light abrasion caused by the asperities and scratches of the counter-ball, this last evident in the OM image shown in Fig. 5E. In turn, this shows that, with its ultra-high hardness, the $1B_4C–1SiC–1TiB_2$ composite also slightly wore the more also-ultrahard diamond-coated SiC counter-ball, so that both lightly abraded each other. Interestingly, there is also evidence of the formation of a coherent tribolayer (*i.e.*, continuous and well-adhered) on the wear track of the $1B_4C–1SiC–1TiB_2$ composite (Figs. 5C-D), but not on the wear scar of the counter-ball (Fig. 5E). The detailed EDS analyses of the tribolayer, such as the

elemental-O map shown by way of example in Fig. 5F, demonstrate that it is of oxide nature, whose formation is therefore attributable to the oxidation of the contact zone as a consequence of the frictional heating generated during the wear tests in air atmosphere. Moreover, higher-magnification SEM images of the regions with material removal, such as the one shown by way of example in Fig. 5G, that this occurred essentially by limited detachment of the oxide tribolayer. Therefore, given its lower shear strength [27] and coherence, the tribolayer must have lubricated and protected the sliding contact, thus adding to the inherent ultra-high hardness of the $1B_4C–1SiC–1TiB_2$ composite to make it so invulnerable to dry sliding wear.

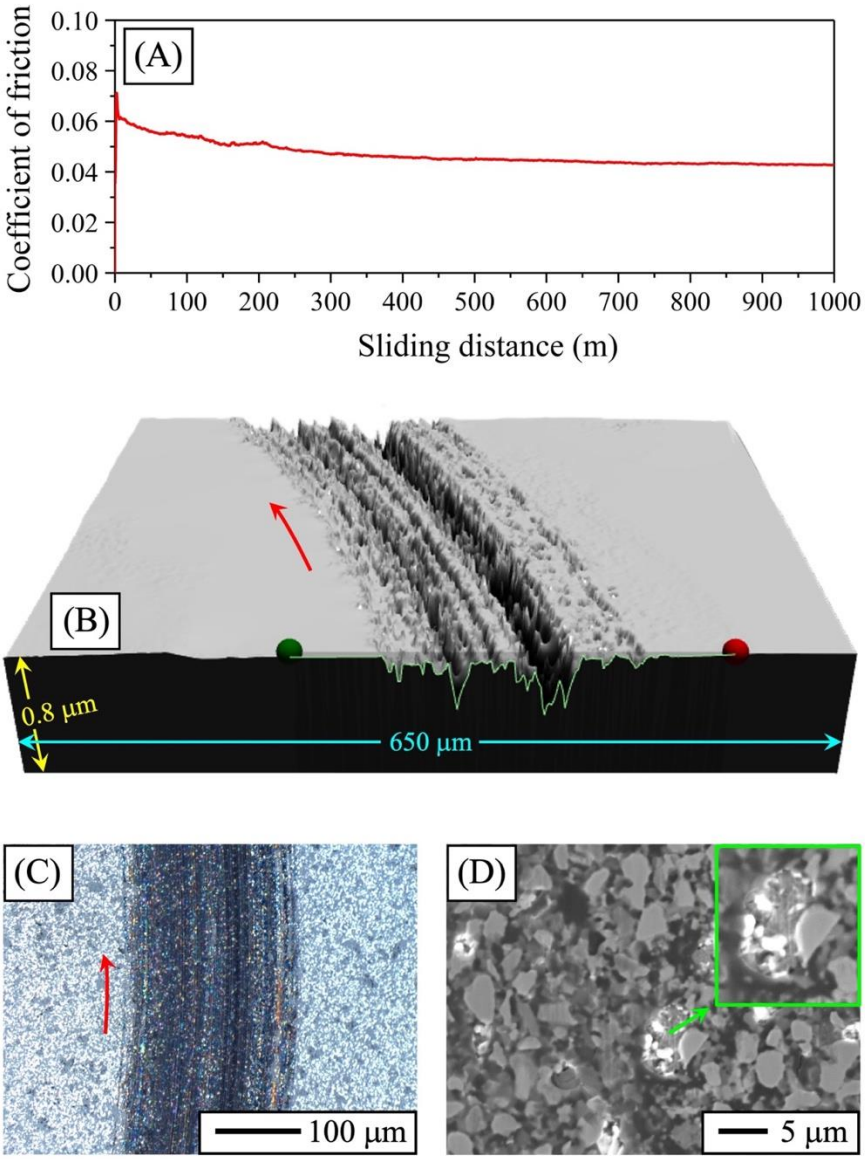

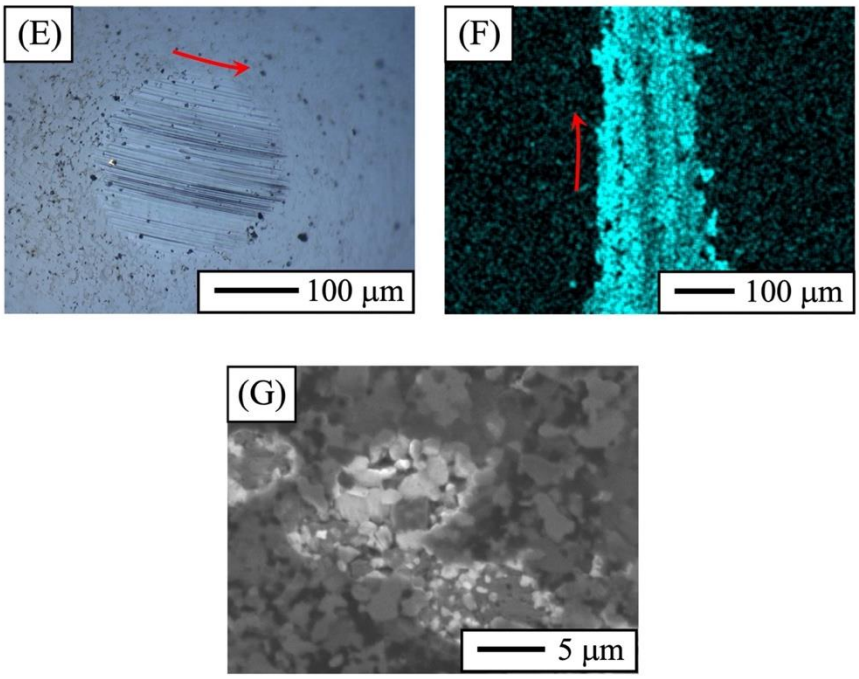

Figure 5. *Set of results deriving from the sliding-wear tests for the optimal $1B_4C–1SiC–1TiB_2$ composite SPS-ed for 5 min under 75 MPa at 1800°C. (A) Friction curve measured as a function of the distance slid, (B) 3-D image and 2-D profile representative of the wear track, obtained by OP, (C) OM image showing the damage at the macro-scale, (D) SEM image showing the damage at the micro-scale, (E) OM image of the diamond-coated SiC counter-ball showing its damage, (F) elemental composition map of O inside and outside the wear track, obtained by EDS, and (G) higher-magnification SEM image showing details of the material removal. The arrow in (B)-(F) marks the sliding direction. Imaging (OP, OM, and SEM/EDS at 10 kV with secondary electrons) was done at the conclusion of the wear tests after cleaning the worn surfaces.*

In general, B_4C–based materials are all, if sufficiently dense, highly wear resistant. That said, it is also true that earlier tribological studies performed under identical testing conditions (*i.e.*, at 40 N load, 1000 m sliding distance, 2-mm track radius, and 6.02 mm diameter diamond-coated SiC counter-ball) on B_4C SPS-ed without and with either Ti-Al, $MoSi_2$, or Si aids have reported SWRs on the order of 10^{-7}–10^{-8} $mm^3/(N·m)$ [3,4,29-31], which are one or two orders of magnitude greater than the unprecedented SWR of 10^{-9} $mm^3/(N·m)$ measured here for the present $1B_4C–1SiC–1TiB_2$ composite, attributable to the latter either being more ultrahard and/or having greater

proneness to form a coherent oxide tribolayer than the former. Certainly, when also tested tribologically under 40 N load, and a B_4C composite SPS-ed at 1800°C with 20 vol.% $MoSi_2$ exhibited a SWR of ~$3.73 \cdot 10^{-8}$ mm³/(N·m) [3], a B_4C composite SPS-ed at 1400°C with 40 vol.% $MoSi_2$ a SWR of ~$4.92 \cdot 10^{-8}$ mm³/(N·m) [4], a B_4C composite SPS-ed at 1800°C with 7 vol.% Ti-Al a SWR of ~$3.1 \cdot 10^{-8}$ mm³/(N·m) [29], a B_4C composite SPS-ed at 1850°C with 5 vol.% Ti-Al a SWR of ~$5.2 \cdot 10^{-8}$ mm³/(N·m) [30], a B_4C composite SPS-ed at 1400°C with 20 vol.% Si a SWR of ~$1.1 \cdot 10^{-7}$ mm³/(N·m) [31], a B_4C composite SPS-ed at 1800°C with 4.28 vol.% Si a SWR of ~$7.3 \cdot 10^{-8}$ mm³/(N·m) [31], and a B_4C monolith SPS-ed at 2100°C a SWR of ~$3.8 \cdot 10^{-8}$ mm³/(N·m) [29]. Consequently, this and other possible B_4C–SiC–TiB_2 composites are even more promising materials for tribological applications than other B_4C–based materials, and they deserve further study under very varied tribological conditions (both model and nominally representative of engineeringly-relevant situations).

4. Conclusions

A study was conducted on the fabrication by solid-state SPS and tribological characterisation of $1B_4C$–1SiC–$1TiB_2$ triplex-particulate ceramic composites. Based on the experimental results and analyses, the following conclusions can be drawn:

1. Solid-state SPS of commercially available B_4C+SiC+TiB_2 powders, blended in equal volume fractions of the three, is optimal at 1800°C. SPS at lower temperature results in porous, and therefore softer, composites, and SPS at higher temperature benefits neither hardness nor toughness of these composites.
2. The optimally SPS-ed $1B_4C$–1SiC–$1TiB_2$ composite has a triplex-particulate microstructure with evenly distributed carbide and boride grains whose sizes are

essentially those of the corresponding starting powders, and is ultrahard (*i.e.*, ~35 GPa) and relatively tough (*i.e.*, ~4 MPa·$m^{1/2}$).

3. The fully dense $1B_4C–1SiC–1TiB_2$ composite has an unprecedented super wear resistance to unlubricated sliding contact (*i.e.*, ~$1.6·10^8$ (N·m)/mm^3), attributable to its ultra-high hardness and proneness to form a coherent oxide tribolayer, undergoing only very mild abrasion in the form of superficial plastic scratches with hardly any material removal by micro-fracture.

Acknowledgements

This work was supported by the Junta de Extremadura under Grants nos. IB20017, TA18014, and GR21170, all co-financed with FEDER Funds.

References

1. W.G. Fahrenholtz, E.W. Neuman, H.J. Brown-Shaklee, G.E. Hilmas, Superhard boride–carbide particulate composites, J. Am. Ceram. Soc. 93 [11] (2010) 3580–3583.
2. C. Ojalvo, F. Guiberteau, A.L. Ortiz, Fabricating toughened super-hard B_4C composites at lower temperature by transient liquid-phase assisted spark plasma sintering with $MoSi_2$ additives, J. Eur. Ceram. Soc. 39 [9] (2019) 2862–2873.
3. V. Zamora, C. Ojalvo, F. Guiberteau, O. Borrero-López, A.L. Ortiz, Ultra-low wear B_4C–SiC–MoB_2 composites fabricated at lower temperature from B_4C with $MoSi_2$ additives, J. Eur. Ceram. Soc. 41 (16) (2021) 68–75.
4. V. Zamora, F. Guiberteau, O. Borrero-López, A.L. Ortiz, Ultra-low temperature spark plasma sintering of super wear-resistant hard B_4C composites, Scripta Mater. 211 (2022) 114516.
5. E.W. Neuman, G.E. Hilmas, W.G. Fahrenholtz, Transition metal diboride-silicon carbide-boron carbide ceramics with super-high hardness and strength, J. Eur. Ceram. Soc. 42 [15] (2022) 6795–6801.
6. L. Hu, Z. Lu, R. He, H. Lei, Z. Qu, Y. Yang, D. Fang, Oxidation behavior of B_4C-(ZrB_2-SiC) ceramics at 1600 °C, Int. J. Refract. Met. Hard Mater. 78 (2019) 282–287.
7. W.S. Rubink, W. Ageh, H. Lide, N.A. Ley, M.L. Young, D.T. Casem, E.J. Faierson, T.W. Schard, Spark plasma sintering of B_4C and B_4C-TiB_2 composites: Deformation and failure mechanisms under quasistatic and dynamic loading, J. Eur. Ceram. Soc. 41 [6] (2021) 3321–3332.
8. Q. He, A. Wang, C. Liu, W. Wang, H. Wang, Z. Fu, Microstructures and mechanical properties of B_4C–TiB_2–SiC composites fabricated by ball milling and hot pressing, J. Eur. Ceram. Soc. 38 [7] (2018) 2832–2840.

9. E.W. Neuman, H.J. Brown-Shaklee, G.E. Hilmas, W.G. Fahrenholtz, Titanium diboride–silicon carbide–boron carbide ceramics with super-high hardness and strength, J. Am. Ceram. Soc. 101 [2] (2018) 497–501.

10. Z. Aygüzer Yaşar, A.M. Celik, R.A. Haber, Improving fracture toughness of B_4C–SiC composites by TiB_2 addition, Int. J. Refract. Met. Hard Mater. 108 (2022) 105930.

11. Y. Liu, X. Wu, M. Liu, Y. Huang, Z. Huang, Microstructure and mechanical properties of B_4C–TiB_2–SiC composites fabricated by spark plasma sintering, Ceram. Int. 46 [3] (2020) 3793–3800.

12. X. Zhang, Z. Zhang, Y. Liu, A. Wang, S. Tian, W. Wang, J. Wang, High-performance B_4C–TiB_2–SiC composites with tuneable properties fabricated by reactive hot pressing, J. Eur. Ceram. Soc. 39 [10] (2019) 2995–3002.

13. X. Zhang, Z. Zhang, W. Wang, J. Shan, H. Che, J. Mu, G. Wang, Microstructure and mechanical properties of B_4C–TiB_2–SiC composites toughened by composite structural toughening phases, J. Am. Ceram. Soc. 100 [7] (2017) 3099–3107.

14. P. He, S. Dong, Y. Kan, X. Zhang, Y. Ding, Microstructure and mechanical properties of B_4C–TiB_2 composites prepared by reaction hot pressing using Ti_3SiC_2 as additive, Ceram. Int. 42 [1 Part A] (2016) 650–656.

15. Z. Zhong, A. Yang, R. Wang, Q. Wen, Z. Zhu, G. Wang, H. Zhang, On the use of Ti–Si eutectic alloy as a novel sintering aid for B_4C–TiB_2–SiC ceramic composites, Ceram. Int. 45 [9] (2019) 12393–12398.

16. Y. Wang, Q. Liu, B. Zhang, H. Zhang, Y. Jin, Z. Zhong, J. Ye, Y. Ren, F. Ye, W. Wang, Microstructure and mechanical behaviour of transient liquid phase spark plasma sintered B_4C–SiC–TiB_2 composites from a B_4C–$TiSi_2$ system, Ceram. Int. 47 [8] (2021) 10665–10671.

17. S.-P. Yin, Z.-H. Zhang, X.-W. Cheng, T.-J. Su, Z.-Y. Hu, Q. Song, H. Wang, Spark plasma sintering of B_4C–TiB_2–SiC composite ceramics using B_4C, Ti_3SiC_2 and Si as starting materials, Ceram. Int. 44 [17] (2018) 21626–21632.

18. Q. Song, Z.-H. Zhang, Z.-Y. Hu, S.-P. Yin, H. Wang, Z.-W. Ma, Microstructure and mechanical properties of super-hard B_4C ceramic fabricated by spark plasma sintering with (Ti_3SiC_2+Si) as sintering aid, Ceram. Int. 45 [7 Part A] (2019) 8790–8797.

19. Y. Liu, H. Liu, Y. Zhou, W. Sha, Y. Huang, Z. Huang, Enhancement mechanical properties of in-situ preparated B_4C–based composites with small amount of (Ti_3SiC_2+Si), Ceram. Int. 48 [9] (2022) 12006–12013.

20. Z.-Y. Hu, Z.-H. Zhang, X.-W. Cheng, F.-C. Wang, Y.-F. Zhang, S.-L. Li, A review A review of multi-physical fields induced phenomena and effects in spark plasma sintering: Fundamentals and applications, Mater. Des. 191 (2020) 108662.

21. X. Wang, N.P. Padture, H. Tanaka, A.L. Ortiz, Wear-resistant ultra-fine-grained ceramics, Acta Mater. 53 [2] (2005) 271–277.

22. P. Chantikul, S.J. Bennison, B.R. Lawn, Role of grain size in the strength and *R*-curve properties of alumina, J. Am. Ceram. Soc. 73 [8] (1990) 2419–2427.

23. D.J. Green, An introduction to the mechanical properties of ceramics, Cambridge University Press, Cambridge, UK, 1998.

24. G.R. Anstis, P. Chantikul, D.B. Marshall, B.R. Lawn, A critical evaluation of indentation techniques for measuring fracture toughness: I direct crack measurement, J. Am. Ceram. Soc. 64 [9] (1981) 533–538.

25. B.M. Moshtaghioun, A.L. Ortiz, D. Gómez-García, A. Domínguez-Rodríguez, Toughening of super-hard ultra-fine grained B4C densified by spark-plasma sintering via SiC addition, J. Eur. Ceram. Soc. 33 [8] (2013) 1395–1401.

26. G. Stachowiak, A.W. Batchelor, Engineering tribology, 3rd Edition, Elsevier Butterworth-Heinemann, Oxford, UK, 2005.

27. B. Bhushan, Modern tribology handbook, CRC Press, Boca Raton, USA, 2001.

28. K. Adachi, K. Kato, N. Chen, Wear map of ceramics, Wear 203–204 (1997) 291–301.

29. C. Ojalvo, E. Sánchez-González, F. Guiberteau, O. Borrero-López, A.L. Ortiz, Improving the dry sliding-wear resistance of B_4C ceramics by transient liquid-phase sintering, J. Eur. Ceram. Soc. 40 [15] (2020) 15286–5292.

30. C. Ojalvo, V. Zamora, R. Moreno, F. Guiberteau, A.L. Ortiz, Transient liquid-phase assisted spark-plasma sintering and dry sliding wear of B_4C ceramics fabricated from B_4C nanopowders, J. Eur. Ceram. Soc. 41 [3] (2021) 1869–1877.

31. V. Zamora, F.J. Martínez-Vázquez, F. Guiberteau, A.L. Ortiz, Unlubricated sliding wear of B_4C composites spark-plasma sintered with Si aids and of their reference B_4C monoliths, J. Eur. Ceram. Soc. (2022), in press.

Figure Captions

Figure 1. SEM micrographs, taken with secondary electrons at 10 kV with no thermal or chemical etching, representative of the fracture surface of the $1B_4C–1SiC–1TiB_2$ composite SPS-ed for 5 min under 75 MPa at (A) 1600°C, (B) 1700°C, (C) 1800°C, and (D) 1900°C. Pitted zones in (C)-(D) are not pores, but small grains pulled-out during fracture.

Figure 2. SEM micrographs, taken with backscattered electrons at 10 kV with no thermal or chemical etching, representative of the fracture surface of the $1B_4C–1SiC–1TiB_2$ composite SPS-ed for 5 min under 75 MPa at (A) 1600°C, (B) 1700°C, (C) 1800°C, and (D) 1900°C, as well as (E)-(F) of the polished surface of the $1B_4C–1SiC–1TiB_2$ composite SPS-ed at 1800°C.

Figure 3. XRD patterns, acquired with pure $CuK\alpha_1$ incident radiation, of the $1B_4C–1SiC–1TiB_2$ composite SPS-ed for 5 min under 75 MPa at 1600°C, 1700°C, 1800°C, and 1900°C, as indicated. Peak assignations, performed using the PDF2 database, are included. The intensity scale is logarithmic to facilitate observation of the weaker peaks.

Figure 4. Hardness and fracture toughness, determined by Vickers indentation tests, of the $1B_4C–1SiC–1TiB_2$ composite SPS-ed for 5 min under 75 MPa at 1600°C, 1700°C, 1800°C, and 1900°C, as indicated. Mean values and standard deviations of 10 separate tests at 9.8 N are reported.

Figure 5. Set of results deriving from the sliding-wear tests for the optimal $1B_4C–1SiC–1TiB_2$ composite SPS-ed for 5 min under 75 MPa at 1800°C. (A) Friction curve measured as a function of the distance slid, (B) 3-D image and 2-D profile representative of the wear track, obtained by

OP, (C) OM image showing the damage at the macro-scale, (D) SEM image showing the damage at the micro-scale, (E) OM image of the diamond-coated SiC counter-ball showing its damage, (F) elemental composition map of O inside and outside the wear track, obtained by EDS, and (G) higher-magnification SEM image showing details of the material removal. The arrow in (B)-(F) marks the sliding direction. Imaging (OP, OM, and SEM/EDS at 10 kV with secondary electrons) was done at the conclusion of the wear tests after cleaning the worn surfaces.

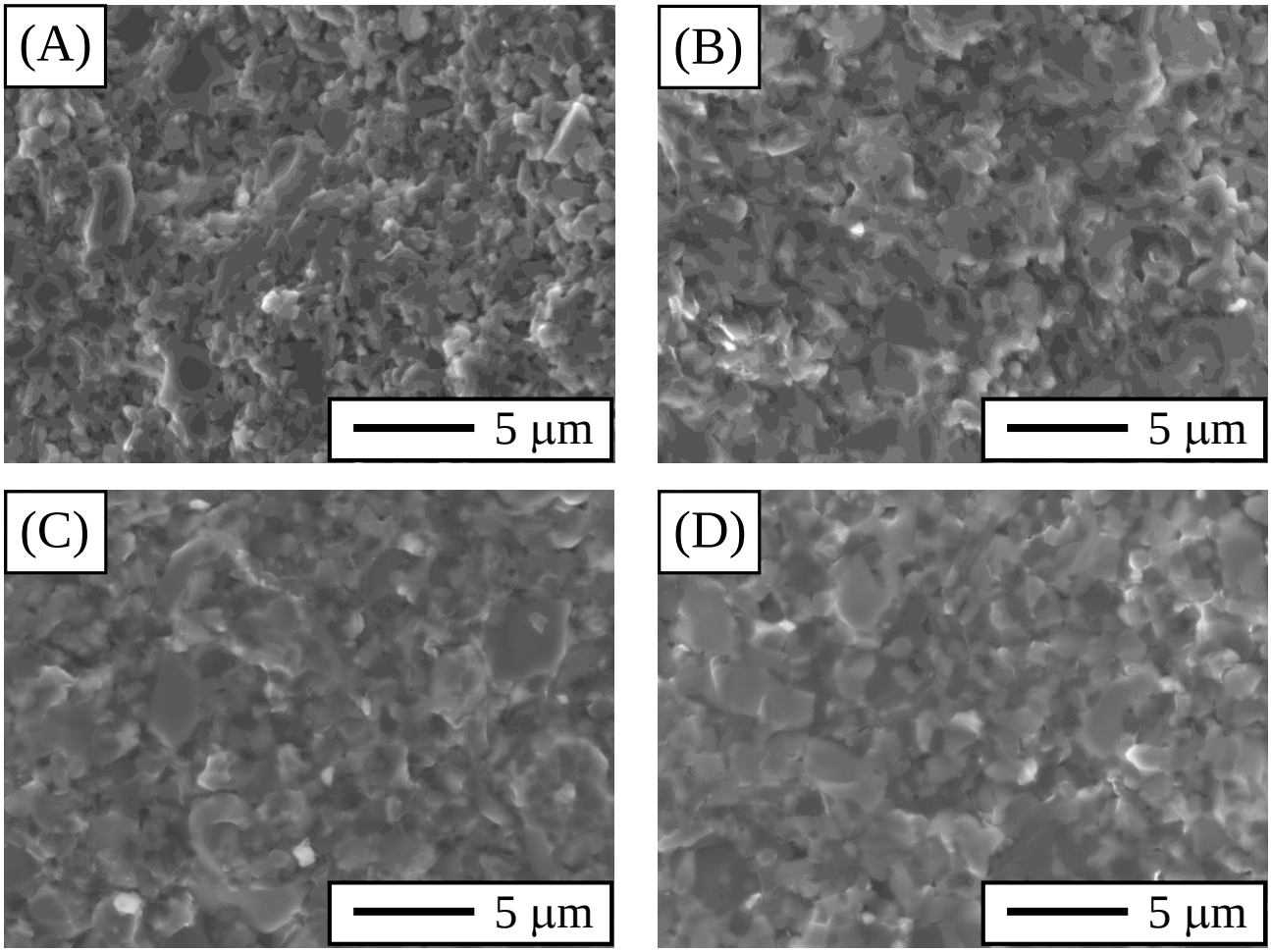

Figure 1

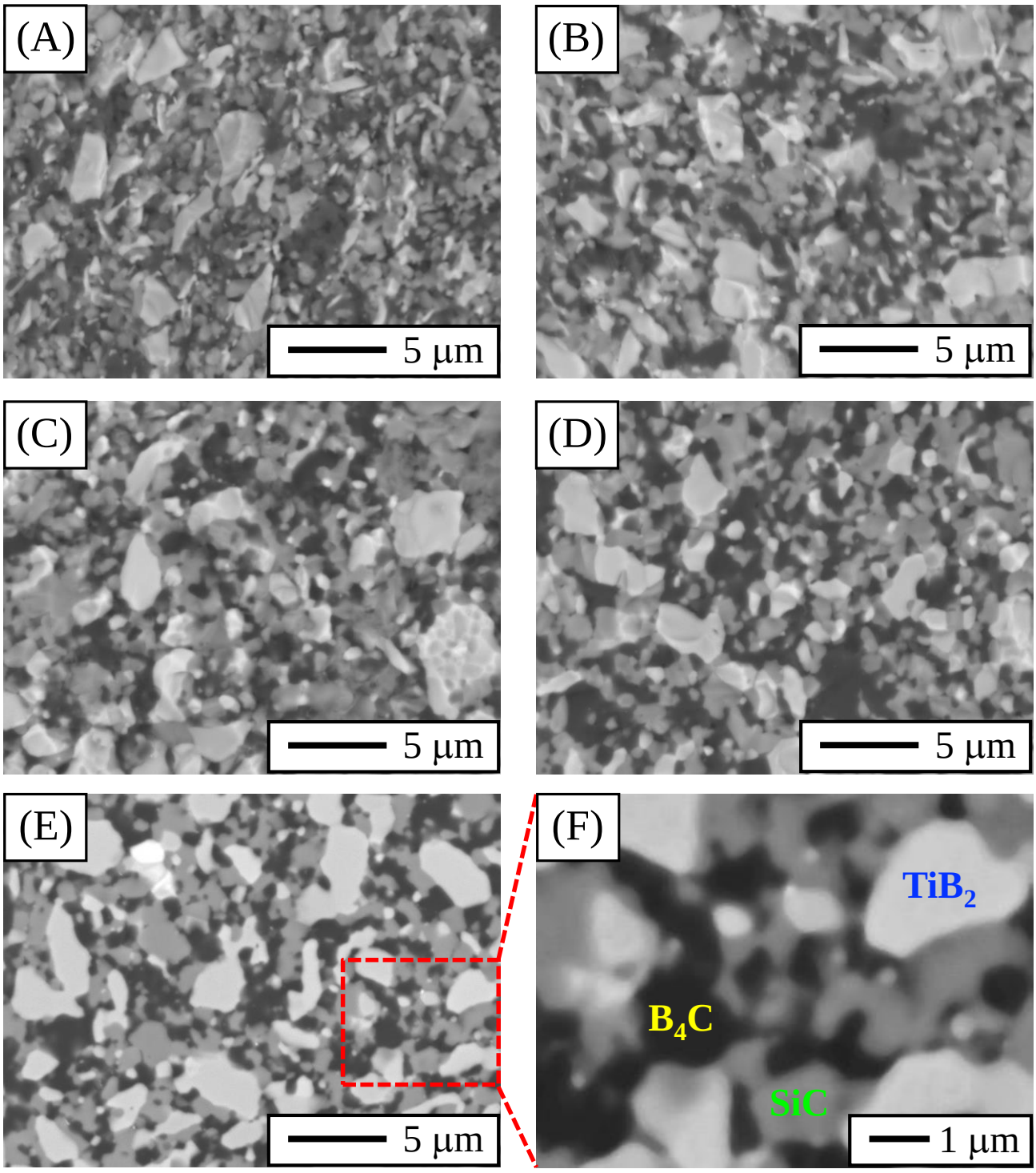

Figure 2

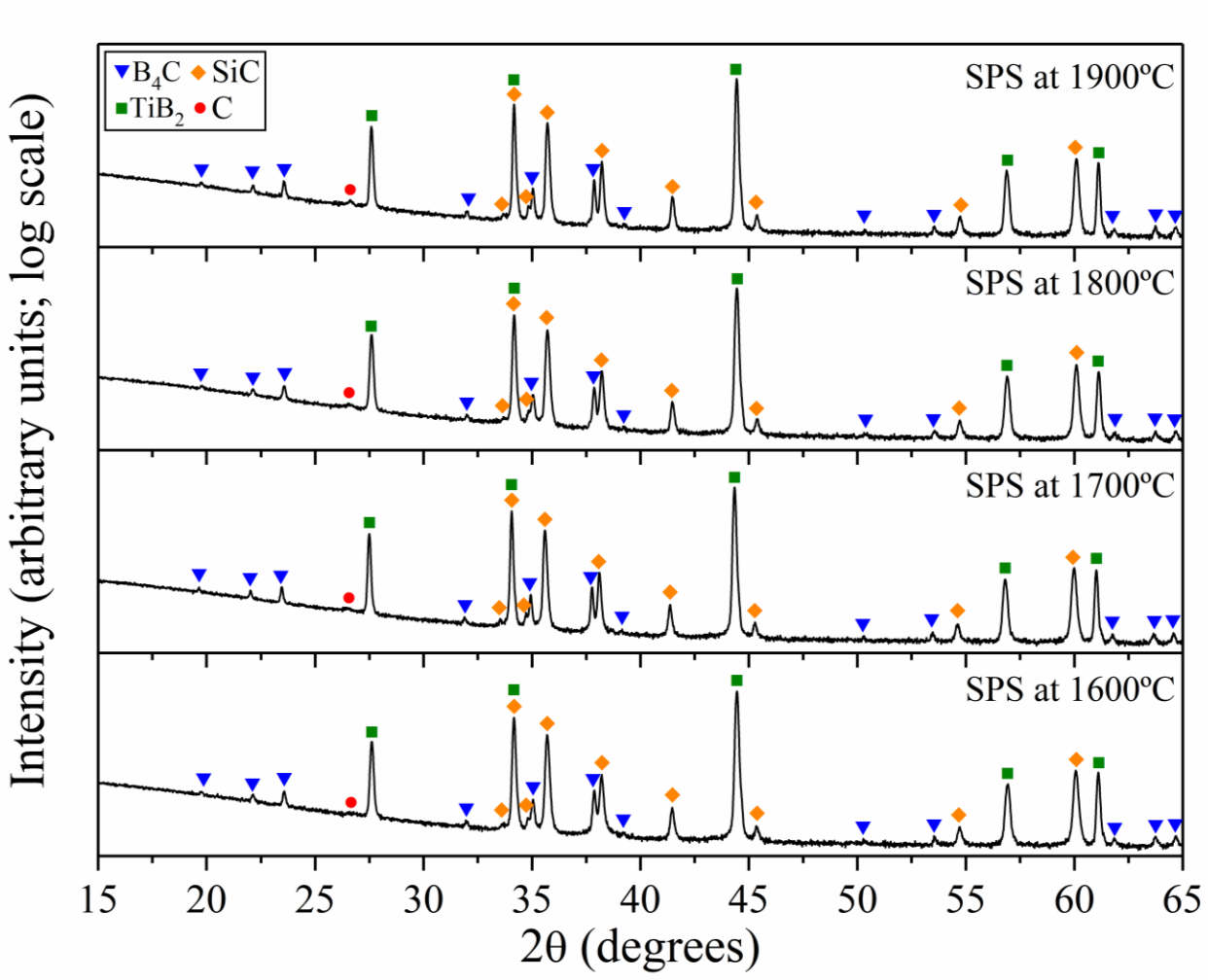
▼B4C ◆SiC
■TiB2 ●C
SPS at 1900ºC
SPS at 1800ºC
SPS at 1700ºC
SPS at 1600ºC
Intensity (arbitrary units; log scale)
15
20
25
30
35
40
45
50
55
60
65
2θ (degrees)

Figure 3

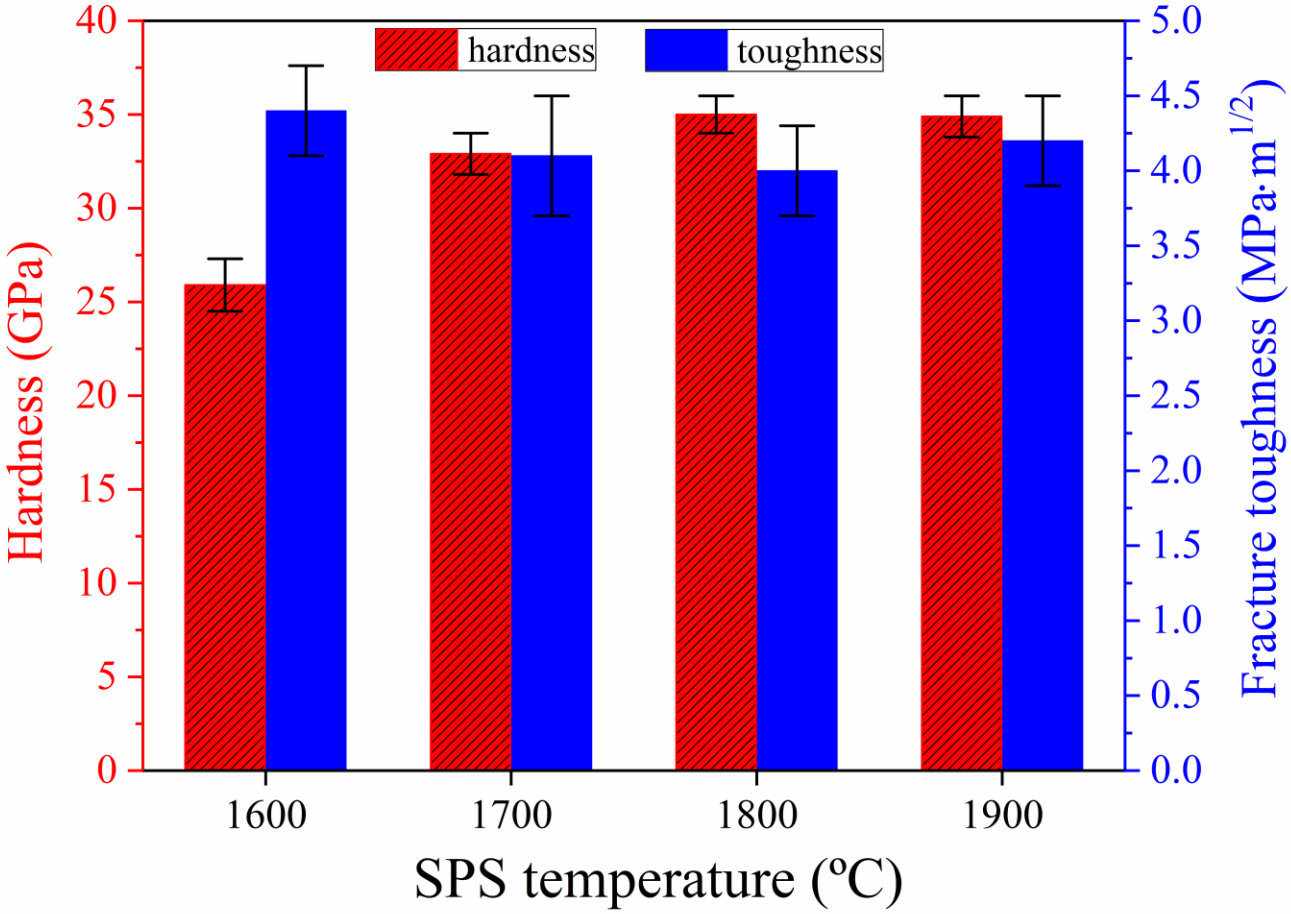
hardness
toughness
Hardness (GPa)
Fracture toughness (MPa·m$^{1/2}$)
SPS temperature (ºC)
0
5
10
15
20
25
30
35
40
0.0
0.5
1.0
1.5
2.0
2.5
3.0
3.5
4.0
4.5
5.0
1600
1700
1800
1900

Figure 4

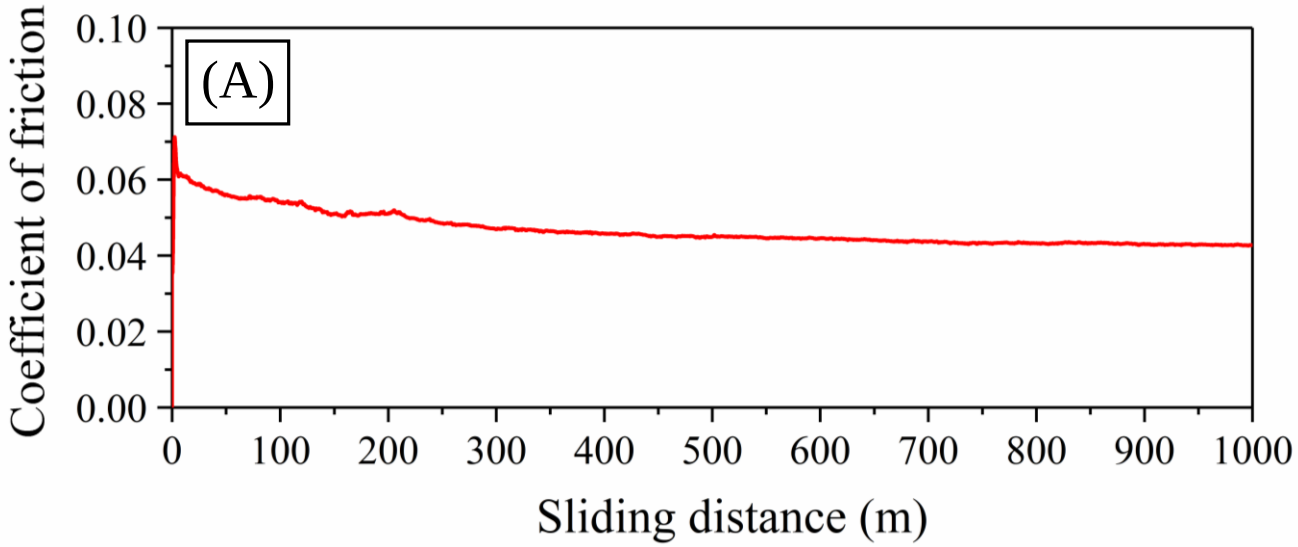
(A)
Coefficient of friction
0.10
0.08
0.06
0.04
0.02
0.00
0
100
200
300
400
500
600
700
800
900
1000
Sliding distance (m)

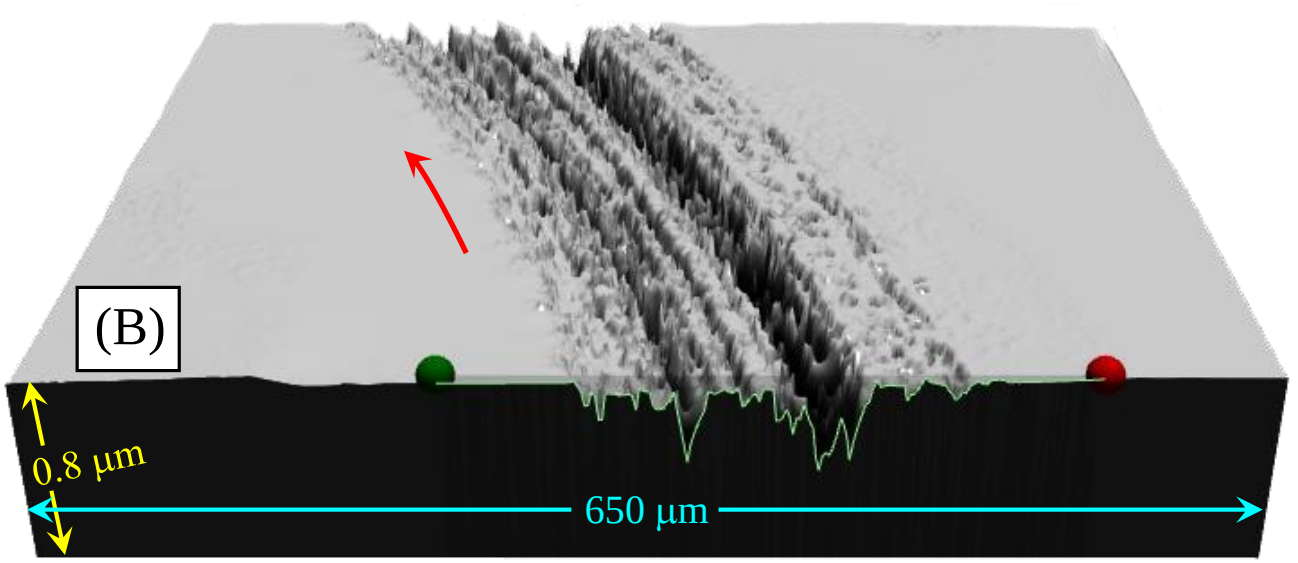
(B)
0.8 µm
650 µm

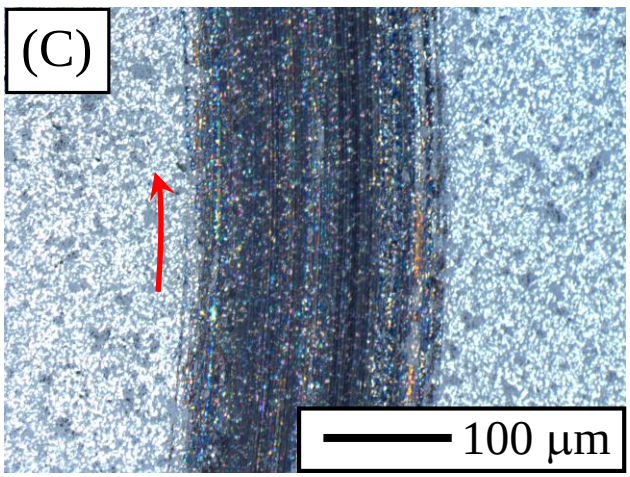
(C)
100 µm

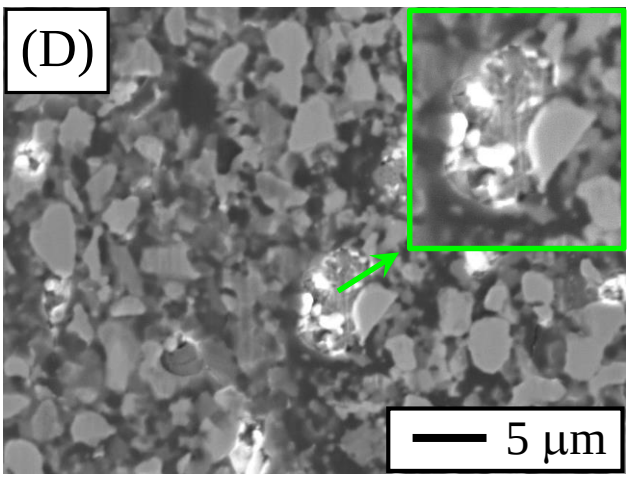
(D)
5 µm

Figure 5

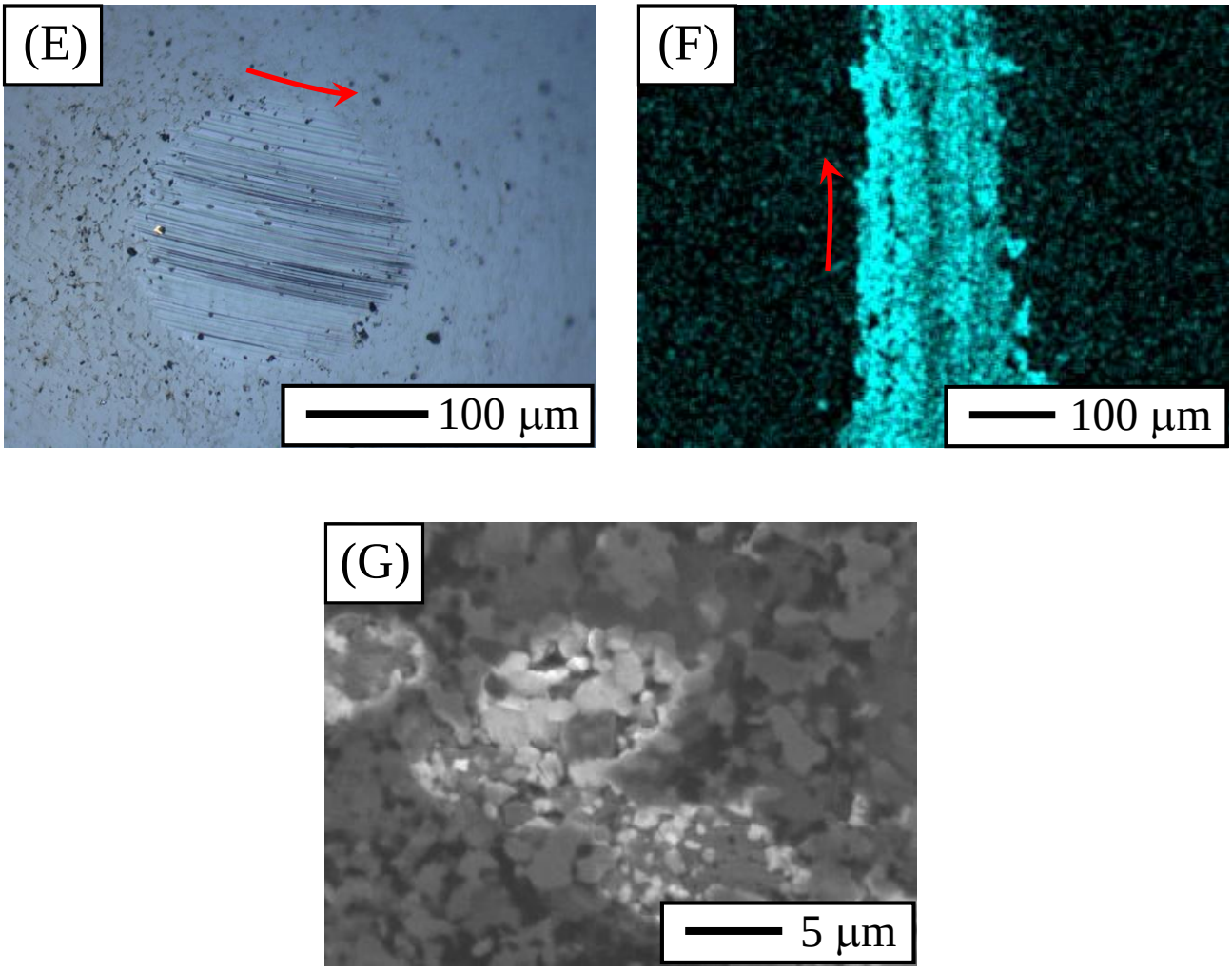

Figure 5